AVIRIS-3 Rapid Response to January 2025 Los Angeles Wildfires

Megan Ward-Baranyay[1,2†], Red Willow Coleman[1,3†], Mark Wronkiewicz[1], Francisco Ochoa[1,3], Daniel Sousa[2], Ceth W. Parker[1], David R. Thompson[1], Clayton D. Elder[4], Gregory S. Okin[3], K. Dana Chadwick[1], Kimberley Miner[1], John Chapman[1], Regina Eckert[1], Daniel Jensen[1], Robert O. Green[1], Philip G. Brodrick[1]

[1]Jet Propulsion Laboratory, California Institute of Technology, Pasadena, CA
[2]Department of Geography, San Diego State University, San Diego, CA
[3]Department of Geography, University of California, Los Angeles, Los Angeles, CA
[4]Earth Science Division, NASA Ames Research Center, Moffett Field, CA
† Authors contributed equally to this study

Key Points:

- Demonstration of rapid structural damage assessment with airborne imaging spectroscopy over a wildland-urban interface (WUI) fire
- Char/ash fractional cover estimated with a generic spectral endmember library is effective for rapid wildfire structural damage assessment
- Localized urban spectral endmember library collected post-fire *in situ* increases the accuracy of structural damage assessment

Corresponding author: Philip G. Brodrick, philip.brodrick@jpl.nasa.gov

Abstract

Wildfires in wildland-urban interfaces (WUIs) are a growing concern due to their devastating impact on human communities and ecosystems. Low-latency impact assessment is critical for wildfire response, yet immediate access to fire-affected communities can be limited. Here, we demonstrate that unmixing char/ash fractional cover using imaging spectroscopy data can support rapid structural damage assessment. Using acquisitions over the 2025 Eaton Fire burn scar collected by the Airborne Visible/Infrared Imaging Spectrometer 3 (AVIRIS-3), we demonstrate that a generic spectral endmember library is sufficient for binary structural damage classification between undamaged and destroyed buildings with an accuracy of 86.3%. Incorporating locally collected Eaton Fire endmembers into the library improves the accuracy by 1.3%. This demonstrates the feasibility of assessing structural damage from airborne imaging spectroscopy to rapidly inform post-fire response and recovery efforts in WUI communities.

Plain Language Summary

Rapid assessment of wildfire structural damage in densely populated neighborhoods is critical. Within days of ignition, imaging spectroscopy data were acquired by the Airborne Visible/Infrared Imaging Spectrometer (AVIRIS-3) over the January 2025 Eaton Fire in Los Angeles County, CA. We demonstrate that it is possible to distinguish between fire-destroyed and undamaged structures by mapping the distribution of char and ash in the aftermath of the Eaton Fire using AVIRIS-3 data. Structural damage classification with an accuracy of 86.3% was achieved without requiring local char and ash sampling. This is critical given that local sample collection can be challenging due to limited accessibility to burned areas. This advance suggests that airborne imaging spectroscopy can be applied for timely, preliminary structure-level damage classification in a wildland-urban interface community.

1 Introduction

Wildfire is a complex natural process and potential hazard where multiple natural climatic, land cover, and hydrological factors drive spatiotemporal patterns and behavior, and is strongly influenced by anthropogenic activity (Abatzoglou & Williams, 2016; Duane et al., 2021). Wildfires in the Wildland-Urban Interface (WUI), which occur when structures are built in or near wildland vegetation, are particularly concerning due to their destructive impact on human communities and ecosystems (Radeloff et al., 2018). The frequency and intensity of wildfires are increasing, including those at the urban interface, driven by anthropogenic climate change, increased urbanization, altered ecosystem management practices, and a history of fire suppression (Radeloff et al., 2018; Tang et al., 2024). Therefore, wildfires demand novel, rapid-response protocols to assess wildfire damage and hazards and to inform first responders (Swain et al., 2025). On 7 January 2025, several wildfires began in Los Angeles County during a Santa Ana wind event, including the Eaton and Palisades Fires, which quickly spread to highly populated urban areas (Wall et al., 2025) [Figure 1A]. This paper focuses on the Eaton Fire in Altadena, Pasadena, and Sierra Madre, CA. Approximately 14,000 acres burned in the Eaton Fire, resulting in 18 fatalities and over 9,400 structures destroyed (Wall et al., 2025; CALFIRE, 2025b). This tragic event was emblematic of the growing threat of WUI fires that result in significant loss of life and property due to the direct interaction between human development and the natural landscape (Radeloff et al., 2018; Swain et al., 2025; Wall et al., 2025).

Imaging spectroscopy (also known as hyperspectral) data are valuable for monitoring pre-fire fuel load, active fire, and post-fire effects (Veraverbeke et al., 2018). Airborne imaging spectroscopy is particularly well-suited to fire monitoring, given its deployment versatility, quick response time, and high spatial resolution relative to orbital

instruments. Previous work has established the utility of imaging spectroscopy for wildfire applications, including fire detection (Dennison & Roberts, 2009), fire temperature estimation (Dennison et al., 2006), post-fire land cover mapping (Tane et al., 2018), and burn severity mapping (van Gerrevink & Veraverbeke, 2021). However, few studies have specifically explored the applications of imaging spectroscopy in WUI fires. This manuscript investigates this potential using NASA Jet Propulsion Laboratory's Airborne Visible/Infrared Imaging Spectrometer 3 (AVIRIS-3), a visible-to-shortwave (VSWIR) spectrometer that covers a spectral range of 390-2500 nm with a spectral sampling of approximately 7.4 nm and flight altitude-dependent spatial resolution (Green, Schaepman, et al., 2022). AVIRIS-3 is a science-grade imaging spectrometer with a design and performance similar to that of the EMIT spectrometer onboard the International Space Station (Thompson et al., 2024). The wildfire science and applications using airborne imaging spectroscopy described in this paper are vital for preparing for future orbital imaging spectroscopy missions and global wildfire rapid response applications, including the proposed NASA Surface Biology and Geology (SBG) mission (Cawse-Nicholson et al., 2021).

Airborne imaging spectrometers have the potential to play a unique role in mapping active and post-fire burned areas. However, there are few instances where airborne data have been obtained over severe, WUI fires. In response to the January 2025 Los Angeles wildfires, AVIRIS-3 was used to help fill in this knowledge gap by mapping the Los Angeles fires both during and after the fires. The spatial resolution of the AVIRIS-3 imagery acquired over the Eaton Fire varied between 1.8 m and 2.8 m, providing dozens of pixels per structure. This study demonstrates that analyzing AVIRIS-3 pixels within building footprints enables automatic classification of structural damage (i.e., burned or not burned). For wildfire incidents in densely populated WUI zones, differentiating damaged from undamaged structures can be challenging, costly, and potentially hazardous in the immediate aftermath of a fire, highlighting the need for reliable, quantitative damage assessments from remotely sensed data In this work, we demonstrate the capability of airborne imaging spectroscopy to quantify structural damage, which has the potential to be used in future disaster response scenarios.

2 Methods

2.1 AVIRIS-3 Flights

Before, during, and after the 2025 Los Angeles wildfires, AVIRIS-3 was deployed on a B200 King Air to collect imaging spectroscopy data on 11, 15, and 23 January 2025. While the flights prior to the fires were serendipitous, during and post-fire acquisitions were obtained with the goal of aiding research into disaster response. Data from all three of these time periods were published as part of the facility instrument radiance (Eckert et al., 2024) and reflectance (Brodrick, Chlus, et al., 2025) data collections. Figure 1A shows the different fires that were mapped, and Figure 1C indicates the different flight directions on different days. For this analysis, we focus primarily on the data from 16 January 2025, which was the clearest early post-fire dataset, and limit our analysis to the vicinity of the Eaton fire.

2.2 AVIRIS-3 Char/Ash Fraction Mapping

Spectral unmixing for sub-pixel image analysis enables the mapping of the fractional cover of post-fire surface materials, such as char and ash (Quintano et al., 2023). Figure 1B shows a surface char/ash fractional (CAF) abundance map produced from AVIRIS-3 imaging spectroscopy orthocorrected surface reflectance measurements for imagery acquired over the Eaton Fire on 11 and 16 January 2025. AVIRIS-3 surface reflectance (Brodrick, Chlus, et al., 2025) was estimated from calibrated radiance measurements using the Optimal Estimation technique adapted for imaging spectroscopy (Thompson et al., 2018), as implemented via the Imaging Spectrometer Optimal FITting codebase (ISOFIT)

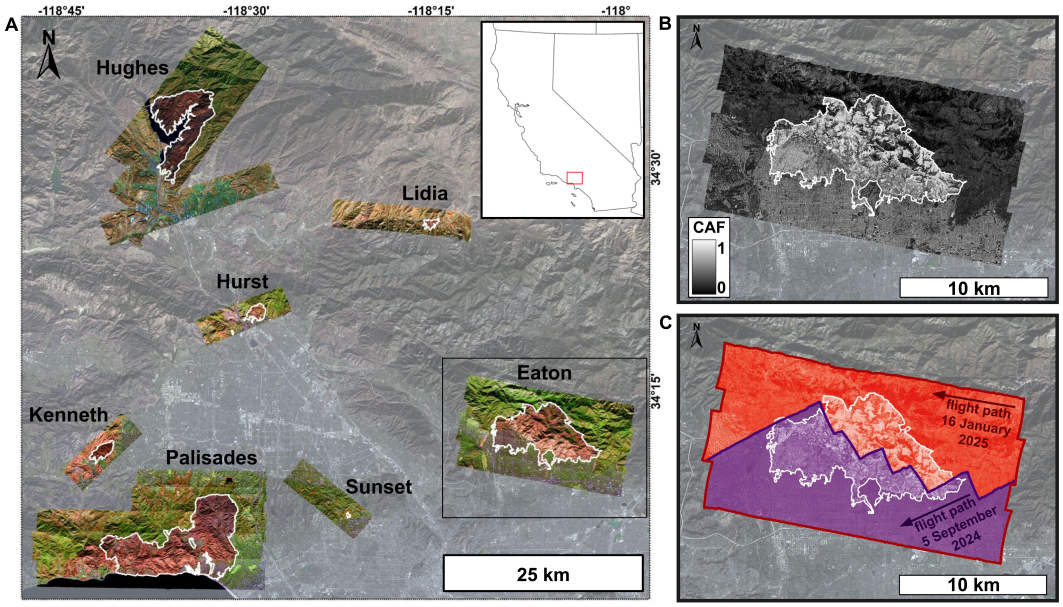

Figure 1. A. False-color visualization (1660nm, 850nm, and 560nm for Red, Green, and Blue, respectively) of AVIRIS-3 acquisitions over seven concurrent Southern California wildfires on 11, 16, and 23 January 2025. Two overpasses were acquired over the Eaton Fire on both 11 and 16 January 2025. The black box contains the extent for B and C. B. Char/Ash fraction (CAF) map on a scale from 0 to 1 (unitless) from AVIRIS-3 imagery over the Eaton Fire. The Eaton Fire perimeter is outlined in white. C. Multiple overflights displayed with pre-fire imagery acquired on 5 September 2024 in purple overlapping post-fire imagery acquired on 16 January 2025 in red. The flight line directions were at an oblique angle to one another. While the pre-fire imagery did not cover the entire Eaton Fire perimeter, only 18 of the affected structures were not captured in the pre-fire imagery. The basemaps for A, B, and C are from Landsat 8 imagery acquired on 16 January 2025.

(Brodrick et al., 2024). Reflectance spectra were brightness-normalized using the root-mean-square of all included wavelengths. Only wavelengths in the ranges 440-1310 nm, 1490-1770 nm, and 2050-2440 nm were used to mitigate retrieval discrepancies and calibration artifacts. Multiple Endmember Spectral Mixture Analysis (MESMA) was performed first using a spectral endmember library comprised of burned and unburned endmembers to determine the fraction of char and ash within each pixel. MESMA models each spectrum as a linear combination of endmembers from a spectral library while permitting variation in the number and types of endmembers per pixel (Roberts et al., 1998). MESMA was implemented through the SpectralUnmixing.jl package (Brodrick, Ochoa, et al., 2025).

Two methods were tested for estimating the fractional cover of char/ash within the Eaton Fire burn scar: generic CAF and localized CAF. The generic CAF utilized a generic endmember library of Southern California urban and wildland environments collected before the fire, as well as wildland char/ash endmembers. Localized CAF used a localized endmember library consisting of the aforementioned generic endmembers, plus an additional subset of local char/ash endmembers collected within and downwind of the Eaton Fire burn scar [Table S1]. Within each library, endmembers were categorized as either burned (40 generic and 10 localized endmembers) or unburned (36 generic endmembers) [Figure S1]. AVIRIS-3 imagery was unmixed using MESMA with the generic

library and separately with the localized library to estimate a per-pixel CAF value. A differenced char/ash fraction (dCAF) product was produced by unmixing an AVIRIS-3 image acquired before the fire on 5 September 2024 [Figure 1C] using the same generic endmember library and subtracting the pre-fire fractions from the classified post-fire imagery in an attempt to resolve any urban areas that could be misclassified as char/ash due to complex urban spectral features. We note that potential limitations of the dCAF method arise from the use of both pre-fire and post-fire airborne data, including inconsistencies in spatial resolution and slight terrain-related geolocation mismatch between the AVIRIS-3 acquisition dates.

The generic endmember library contains spectral endmembers collected from urban areas and wildfire-affected wildlands in Southern California. The burned endmembers are char/ash samples from the Lake Fire, collected soon after fire containment in August 2024 using an Analytical Spectral Devices (ASD) FieldSpec 4 spectrometer and contact probe. The Lake Fire primarily burned in minimally developed areas, so this dataset only includes burned soil and vegetation. Unburned endmembers include previously-acquired measurements of roofing tile, paint, asphalt, soil, photosynthetic vegetation (PV), and non-photosynthetic vegetation (NPV) in urban areas (Roberts et al., 2017). Importantly, the local endmember library was expanded to include additional samples collected inside and outside the Eaton Fire perimeter. The sampling protocol yielded nearly 100 char/ash samples, which were subsequently measured using an ASD and a contact probe in a lab (Wronkiewicz et al., 2025). The inclusion of specific endmembers in the smaller, localized library was determined using a convex hull dimensionality reduction strategy to ensure spectral diversity (Ochoa, Brodrick, Okin, Ben-Dor, et al., 2025).

2.3 Ground-Reference Structural Damage Maps

The California Department of Forestry and Fire Protection (CAL FIRE) provides a publicly accessible database of all structures impacted by a wildland fire within 100 meters of a fire perimeter (CALFIRE, 2025a). These data are referred to as the Damage Inspection (DINS) product, reflecting on-the-ground damage assessments by CAL FIRE specialists that provide information on structure type, construction features, and defensible space attributes, as available (Schmidt, 2020; Syphard & Keeley, 2019). The DINS estimates the percentage of a structure that is damaged, with five categories: no damage, 1-9% affected, 10-25% minor damage, 26-50% major damage, and 50-100% destroyed. Structures inaccessible to DINS teams were not categorized. These inspections are intensive and require 360° inspections of each accessible structure. For a more comprehensive description of how CAL FIRE collects and validates DINS data, interested readers are referred to a technical note developed after the 2018 Camp Fire in Paradise, CA (Maranghides et al., 2020). CAL FIRE incident response teams completed the initial DINS data release for the Eaton Fire in late January 2025, providing a parcel-by-parcel structural damage estimate in and near the burn scar.

2.4 Char/Ash Fraction Structural Damage Assessment

We used the CAL FIRE DINS product to validate the AVIRIS-3 CAF and dCAF binary classification of structural damage for the most extreme DINS damage labels ("No Damage" and "Destroyed") across the Eaton Fire burn scar. To link the AVIRIS-derived products with the structural damage estimates, a spatial join was performed between the Los Angeles County Open Street Map (OSM) building footprints and CAL FIRE DINS product (OpenStreetMap contributors, 2025; CALFIRE, 2025a). The pre- and post-fire AVIRIS-3 acquisitions covered 7,773 structures classified as "Destroyed" and 7,151 classified as "No Damage" in the DINS database. The high spatial resolution of AVIRIS-3 imagery acquired over the Eaton Fire (1.8 m to 2.8 m) meant that each structure contained multiple pixels, enabling per-structure averaged estimates of CAF cover. We calculated the median CAF value from pixels intersecting with the polygon corresponding

to each building's footprint, and then applied a binary classifier of structural damage (damaged or undamaged) [Figure 2].

While the CAF metric was not intended as a direct binary classifier of damage, we hypothesize that an increase in CAF is correlated with higher damage rates. To investigate this, we explored how different CAF thresholds result in different damage classifications, following the framework of a Receiver Operating Characteristic (ROC) curve, using the DINS product as a validation set (Hanley & McNeil, 1982; Kerekes, 2008; Wolter & Townsend, 2011). The area under the ROC curve (AUC) provides a general measure of performance when using CAF as a binary classifier of building damage. A higher AUC value indicates that, on average, per-structure median CAF values are higher for destroyed structures relative to undamaged structures. More critically, however, the ROC curve illustrates the tradeoff between the true positive rate (TPR), which represents the probability of correctly classifying a destroyed structure, and the false positive rate (FPR), which denotes the probability of incorrectly classifying an undamaged structure as destroyed. We computed an ROC curve for each CAF metric: local endmember CAF, generic endmember CAF, and dCAF. To evaluate the consistency of the ROC-AUC and the classification accuracy for each CAF metric, we leveraged bootstrapping with 10,000 iterations. In each iteration, we randomly generated a 90/10 train/test split of the data and computed the AUC on a 10% held-out test set. We then assessed the accuracy by using the 90% training set to generate an ROC curve, computing the CAF threshold corresponding to the 10% FPR threshold, and applying this threshold to the held-out test set to generate binary predictions. The CAF value that yielded 10% FPR was 60.3%. The same random data splits were used when assessing each CAF metric. Finally, we computed the mean and standard deviation of the AUCs and accuracies across all iterations.

3 Results

An exploratory data analysis of the AVIRIS-3 CAF product provided confidence that airborne imaging spectroscopy can be used to assess post-fire structural damage. Figure 3 showed that DINS damage severity was generally correlated with a higher CAF, particularly pronounced for the structures categorized as Destroyed. For the generic CAF estimate, the median CAF was 0.51 for undamaged structures and 0.77 for damaged structures. AVIRIS-3 imagery acquired four and nine days post-ignition had a similar median CAF, demonstrating the method's usefulness near-immediately post-fire and its consistency for several days afterward. These results were further quantified using ROC-AUC scores in Figure 4. The local post-fire and generic CAF estimates had similar trends and exhibited the ability to distinguish between destroyed and undamaged structures in the Eaton Fire area. We found that our retrieval was unstable across time points using the dCAF method due to differences in spatial resolution and slight terrain-related geolocation mismatches between the pre-fire and post-fire AVIRIS-3 data.

We used both the ROC-AUC and accuracy to quantify classification performance generally, as well as at a specific cutoff threshold that would be needed to apply the classifier in a realistic scenario aimed to limit false damage reports (FPR = 10%). We find that for both performance measures, the local CAF metric outperforms the generic CAF and dCAF. Its ROC-AUC value of 0.931 was better than generic CAF and dCAF by 0.007 and 0.039, respectively. Similarly, the local CAF accuracy of 87.6% was better than generic CAF and dCAF by 1.3% and 6.6%, respectively. While both local and generic CAF metrics performed better than dCAF, our results (and curves in [Figure 4]) indicate that the difference between the two CAF metrics was minimal. By using a bootstrapping approach, we ensured these results were stable; standard deviation in AUC and accuracy was small across all products (approximately 0.0065 to 0.0093), indicating consistent performance across the dataset [Figure 4].

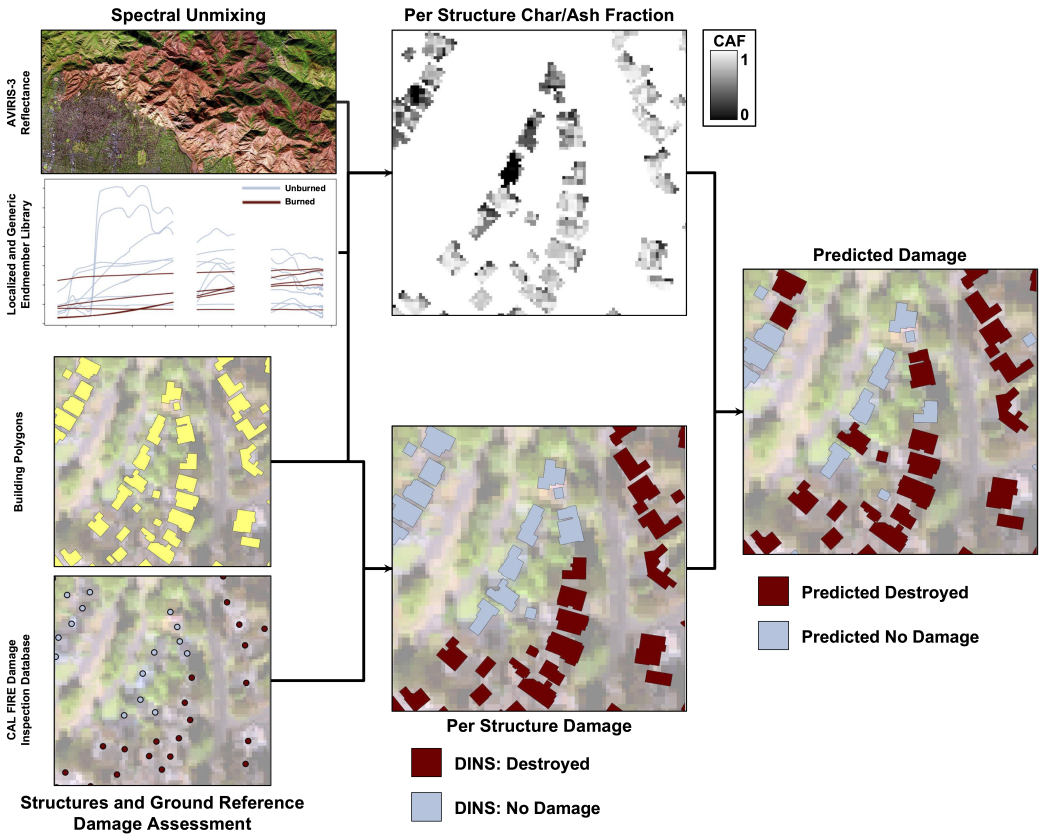

Figure 2. Illustration of the char/ash fractional cover (CAF) product validation. AVIRIS-3 surface reflectance collected over the Eaton Fire was spectrally unmixed using a spectral endmember library where endmembers were categorized as either burned or unburned with a MESMA approach. Endmember library shown depicts a sample of endmembers included in both libraries. See detailed endmember libraries in the supplementary information. The combined Open Street Map building footprints and CAL FIRE DINS products provide a per-structural damage vector dataset with an associated median per-structure CAF. To evaluate prediction accuracy, a CAF threshold was selected on the ROC curve that corresponds to a fixed FPR of 10%. Above that threshold, a structure was predicted as "destroyed."

4 Discussion

In 2025, the Eaton Fire joined a growing list of damaging fires at the wildland-urban interface that have led to fatalities, catastrophic property loss, and whole-neighborhood devastation (Keeley & Syphard, 2019). Within days of fire ignition, AVIRIS-3 acquired multiple overflights of the active fire and post-fire burn scar. This work focused on a small subset of this complex post-fire recovery process: predicting structural damage from airborne imaging spectroscopy data. We developed a rapid turnaround approach derived from airborne spectroscopy data that maps fire structural damage within 48 hours of data on the ground. Low-latency, actionable data are critical for wildfire response, reinforcing the need for optimized pipelines to support decision-makers, as demonstrated by our imaging spectroscopy-derived structural damage assessment (Lee et al., 2022). Spectroscopy-based damage assessment may benefit future wildfire responses by accelerating post-disaster assessment, informing the allocation of resources and deployment of first responders, and identifying areas to prioritize for utility repair. For example, our approach can comple-

ment the manual assessment of structural damage (e.g., DINS), which typically takes days or weeks to complete, by providing a rapid and preliminary evaluation.

4.1 Post-Fire Surface Mapping with Imaging Spectroscopy

The AVIRIS-3 CAF spectral unmixing approach extends earlier research using airborne imaging spectroscopy data for post-fire surface mapping in primarily wildland areas. Here, we demonstrate that it is possible to distinguish between damaged and undamaged structures based on per-structure CAF estimates in a post-WUI fire community. Kokaly et al. (2007) demonstrated that AVIRIS-Classic characterized post-fire surface cover and burn severity more effectively than Landsat Enhanced Thermal Mapping (ETM+) data over a wildland fire in New Mexico using a non-local spectral library and the Tetracorder algorithm. Likewise, we found that using a non-local library yielded results similar to those obtained with a localized spectral library. Veraverbeke et al. (2014) showed that a MESMA unmixing strategy with char, PV, NPV, and substrate local endmembers from a Southern California burn scar outperformed multispectral Landsat estimates of post-fire fractional cover and burned fraction. AVIRIS-Classic imagery was also used to assess post-fire vegetation in semiarid shrub/chaparral communities of the Santa Monica Mountains, suggesting that it may be possible to map similar trends in WUI and non-urban vegetation over the next few years of recovery in the Eaton Fire burn scar (Riaño, 2002).

The choice of endmember library (generic vs. localized) selected for unmixing AVIRIS-3 post-fire imagery to generate CAF and dCAF products is an important factor in this research. Post-fire char/ash endmembers from the Lake Fire wildland burn area used in the generic library included both "dark" ash and "light" ash (incomplete and complete combustion, respectively) that consist primarily of burned grass and woodland NPV (Kokaly et al., 2007). In contrast to the Lake Fire endmembers, the local fire endmembers collected from *in situ* samples taken in and around the Eaton Fire burn scar were more heterogeneous, with spectral signatures indicating a mix of NPV, soil, as well as char and ash from burnt vegetation and anthropogenic materials, including buildings, vehicles, and paint. The Eaton Fire samples were collected in the days following the fire from streets and other public spaces, so they likely consist of nearby burned/unburned materials, as well as wind-deposited materials from up to several miles away, due to the strong Santa Ana winds.

We initially expected the local endmember library to outperform the more general wildland/Southern California endmember library. However, MESMA and other spectral unmixing strategies rely on "pure" endmembers that represent a single land cover class (e.g., vegetation or soil (Roberts et al., 1998)), which could explain why the generic library with "purer" endmembers from a wildland fire performed similarly to the localized library with mixed urban char/ash endmembers for estimating CAF in the Eaton Fire. This result is critical for the rapid application of the unmixing strategy utilized here; collecting *in situ* samples and/or spectra from the debris zone requires time and access, both of which are often unavailable during disaster response. Our work suggests that spectroscopy-based damage assessments are not predicated on local endmembers — a finding that implies low-latency damage assessments are possible soon after airborne spectroscopy data become available.

4.2 Future Applications of Post-Fire Damage Assessment

This research demonstrates that a single post-fire AVIRIS-3 airborne acquisition provides sufficient information for a CAF-driven structural damage assessment. The approach builds on previous research efforts that used CAL FIRE DINS to investigate structure survival patterns in several major WUI fires, including the 2017 Tubbs Fire in Santa Rosa, CA (Schmidt, 2023), the 2018 Camp Fire in Paradise, CA (Knapp et al., 2021; Troy

et al., 2022), and many more fires across California (Syphard & Keeley, 2019; Syphard et al., 2022). While these studies did not rely on remotely sensed data, they demonstrated that the DINS is valuable for identifying predictive variables that drive post-fire structural damage (e.g., housing arrangement, building year, vegetation cover). By expanding this validation framework to the airborne remote sensing landscape, we demonstrate a cost-effective and low-latency option for damage assessment in the aftermath of a fire at the wildland-urban interface. Of course, the transferability of this application to other regions or continents should also be investigated, as this study is based on a single wildfire in a WUI area.

The AVIRIS-3 CAF product may help monitor post-fire recovery and investigate public health-related concerns (e.g., lead contamination) for areas within the burn scar. An airborne monitoring network measured lead levels more than 100 times higher than typical levels over 10 miles from the Eaton Fire (Baliaka et al., 2025). Many of the burnt structures in the Eaton Fire were built before the 1978 lead paint ban, increasing the risk of short-term airborne and possibly longer-term soil lead contamination, with serious health implications (Cohan et al., 2009). Future research should investigate whether known contaminants in the Eaton Fire burn scar (e.g., heavy metals, asbestos, and lithium from EV batteries) are detectable in the post-fire AVIRIS-3 surface reflectance data or derived fractional cover products. Rapidly mapping contaminants in urban fires is advantageous for informing first responders and guiding post-fire recovery efforts. Such an approach was used after the September 11th World Trade Center disaster, where AVIRIS was deployed to assess contamination across Manhattan (Clark et al., 2001). Our findings suggest that similar disaster response strategies may be achievable in an urban burn scar.

Several limitations remain in extending this structural damage assessment to future WUI fire events. Critically, the CAF product only considers the exposed surface (visible from an airborne platform) rather than what is underneath. This can lead to overestimating damage in areas where an unburned area covered in ash returns a high burn fraction. The opposite, where damage within structures is underestimated due to intact and undamaged coverings (e.g., a roof), is also possible. Another limitation is the reliance on accurate geolocation, particularly in areas with variable topography, which is common in some WUI areas. Accurate geolocation is necessary for co-registering AVIRIS pixels with building footprints. The accuracy is also limited based on the availability of up-to-date and accurate structure footprint data (e.g., CAL FIRE DINS). More advanced retrievals might be able to explore the time domain and potential for improved accuracy with dCAF. Although there was a mild sensitivity to partial damage fractions (e.g., Figure 3), more investigation is needed to quantify the performance of CAF-based approaches when assessing damage on a continuum rather than the binary assessment used here. Future studies could also explore the specific types of damage that char/ash unmixing is sensitive to. In addition, investigations are needed into structures misclassified by CAF spectral unmixing, as evaluating spectral features in these structures may uncover methods to improve the spectral library or unmixing strategies that lead to better performance.

Looking towards the increasing number of spaceborne spectrometers, recent work using PRISMA has demonstrated successful fire severity and unmixing analysis over a wildland fire in Spain (Quintano et al., 2023). A comprehensive comparison of spaceborne and airborne spectroscopy data over a WUI fire could illuminate how spaceborne data can assess a spatially and spectrally complex burn scar. The results of this study highlight a potential actionable use case for wildfire damage and hazard assessment in WUI areas. This potential will only grow as instruments with regular and frequent revisit intervals (such as the SBG mission) begin operating, allowing for the establishment of a baseline signal even in the presence of phenological variation (Green, Sen, et al., 2022). That is, regular pre- and post-fire fuel mapping, temporal analysis of background spectra, and coarse risk assessments are all made possible from a regular cadence of space-

borne data. While per-structural damage assessment will be limited with coarser spaceborne spatial data, partial damage fraction estimates will grow in importance and will likely still provide valuable pre-fire and post-fire analyses.

5 Conclusion

Airborne imaging spectroscopy data collected before, during, and after the January 2025 Los Angeles wildfires, now openly available, supports research and applications spanning the disaster response, fire modeling, and imaging spectroscopy communities. We quantified the performance of imaging spectroscopy from AVIRIS-3 for providing an immediate assessment of wildfire structural damage. Furthermore, accurate structural damage estimation was demonstrated using generic, pre-existing spectral endmember libraries. Together, this work suggests that preliminary structural damage maps are not predicated on *in situ* samples, enabling immediate damage assessment from airborne remote sensing data and reducing human exposure to hazards in recently burned urban areas. The dCAF product, which requires both a pre-fire and post-fire image, did not improve structure classification accuracy, suggesting that a single post-fire flight is sufficient for assessing structural damage. Structural damage assessment using airborne imaging spectroscopy can be leveraged in subsequent WUI wildfire disasters as an additional disaster response tool, demonstrating the growing utility of imaging spectroscopy for operational wildfire applications.

Open Research Section

AVIRIS-3 data for the dates and times used in this work are available via the AVIRIS-3 L2A facility instrument collection (Brodrick, Chlus, et al., 2025). Mosaics of char/ash fractions for all dates and times discussed here are available for download Ward-Baranyay et al. (2025). Spectra collected from the 2024 Lake Fire are available for download and use at native resolution (Ochoa, Brodrick, Okin, Roberts, et al., 2025). Spectral unmixing to estimate char/ash fractional cover was computed using the open-source SpectralUnmixing.jl software package (Brodrick, Ochoa, et al., 2025).

CRediT Author Statement

PGB and DRT conceived the study. MWB, RWC, PGB, MW, FO, DS, and DRT analyzed the data. MW, FO, RWC, and CWP obtained field measurements. MWB and RWC wrote the initial draft. ROG and PGB obtained funding to support the work. All authors contributed to the writing of the manuscript.

Conflict of Interest Statement

The authors have no conflicts of interest to disclose.

Acknowledgments

The 2025 Los Angeles fires were a devastating tragedy that deeply affected thousands throughout the region, including several authors of this study. The team wishes to acknowledge and thank the dedicated and incredible efforts of first responders, public officials, and volunteers who worked to minimize the impact of the event.

A portion of this research was carried out at the Jet Propulsion Laboratory, California Institute of Technology, with support from the FireSense program under a contract with the National Aeronautics and Space Administration (80NM0018D0004). DS gratefully acknowledges funding from the NASA (FireSense Program 80NSSC24K0145 and 80NSSC24K1320, and NASA ROSES NNH22ZDA001N-IDS) and the EMIT Science

and Applications Team program (80NSSC24K0861).

References

Abatzoglou, J. T., & Williams, A. P. (2016, October). Impact of anthropogenic climate change on wildfire across western us forests. *Proceedings of the National Academy of Sciences*, *113*(42), 11770–11775. Retrieved from http://dx.doi.org/10.1073/pnas.1607171113 doi: 10.1073/pnas.1607171113

Baliaka, H. D., Ward, R. X., Bahreini, R., Dillner, A. M., Russell, A. G., Seinfeld, J. H., ... Ng, N. L. (2025, February). Notes from the field: Elevated atmospheric lead levels during the los angeles urban fires — california, january 2025. *MMWR. Morbidity and Mortality Weekly Report*, *74*(5), 69–71. Retrieved from http://dx.doi.org/10.15585/mmwr.mm7405a4 doi: 10.15585/mmwr.mm7405a4

Brodrick, P. G., Chlus, A. M., Bohn, U. N., Greenberg, E., Montgomery, J., Chapman, J. W., ... Green, R. O. (2025). *Aviris-3 l2a orthocorrected surface reflectance, facility instrument collection.* ORNL Distributed Active Archive Center. Retrieved from https://daac.ornl.gov/cgi-bin/dsviewer.pl?ds_id=2357 doi: 10.3334/ORNLDAAC/2357

Brodrick, P. G., Ochoa, F., Okin, G., Jhalani, V. A., Olson-Duvall, W., Lundeen, S. R., ... Green, R. O. (2025). Spectralunmixing: A general julia package for unmixing spectroscopy data. *Journal of Open Source Software*, *10*(116), 9149. Retrieved from https://doi.org/10.21105/joss.09149 doi: 10.21105/joss.09149

Brodrick, P. G., Thompson, D. R., Bohn, N., Carmon, N., Eckert, R., Montgomery, J., ... Vaughn, N. (2024). *isofit.* Zenodo. Retrieved from https://zenodo.org/doi/10.5281/zenodo.13968342 doi: 10.5281/ZENODO.13968342

CALFIRE. (2025a). *Cal fire damage inspection (dins) data.* California Department of Forestry and Fire Protection (CAL FIRE). Retrieved from https://data.ca.gov/dataset/cal-fire-damage-inspection-dins-data ([Data set])

CALFIRE. (2025b). *Current emergency incidents: Ongoing emergency responses in california, including all 10+ acre wildfires.* California Department of Forestry and Fire Protection (CAL FIRE). Retrieved from https://www.fire.ca.gov/incidents (Accessed 8 October 2025)

Cawse-Nicholson, K., Townsend, P. A., Schimel, D., Assiri, A. M., Blake, P. L., Buongiorno, M. F., ... Zhang, Q. (2021, May). Nasa's surface biology and geology designated observable: A perspective on surface imaging algorithms. *Remote Sensing of Environment*, *257*, 112349. Retrieved from http://dx.doi.org/10.1016/j.rse.2021.112349 doi: 10.1016/j.rse.2021.112349

Clark, R. N., Green, R. O., Swayze, G. A., Meeker, G., Sutley, S., Hoefen, T. M., ... Adams, M. (2001). *Environmental studies of the world trade center area after the september 11, 2001 attack.* Retrieved from http://dx.doi.org/10.3133/ofr01429 doi: 10.3133/ofr01429

Cohan, A. J., Edwards, R. D., Kleinman, M. T., & Dabdub, D. (2009, October). Potential for atmospheric-driven lead paint degradation in the south coast air basin of california. *Environmental Science and Technology*, *43*(23), 8881–8887. Retrieved from http://dx.doi.org/10.1021/es901360j doi: 10.1021/es901360j

Dennison, P. E., Charoensiri, K., Roberts, D., Peterson, S., & Green, R. (2006, January). Wildfire temperature and land cover modeling using hyperspectral data. *Remote Sensing of Environment*, *100*(2), 212–222. Retrieved from http://dx.doi.org/10.1016/j.rse.2005.10.007 doi: 10.1016/j.rse.2005.10.007

Dennison, P. E., & Roberts, D. A. (2009, August). Daytime fire detection using airborne hyperspectral data. *Remote Sensing of Environment*, *113*(8), 1646–1657. Retrieved from http://dx.doi.org/10.1016/j.rse.2009.03.010 doi: 10.1016/

j.rse.2009.03.010

Duane, A., Castellnou, M., & Brotons, L. (2021, April). Towards a comprehensive look at global drivers of novel extreme wildfire events. *Climatic Change*, *165*(3–4). Retrieved from http://dx.doi.org/10.1007/s10584-021-03066-4 doi: 10.1007/s10584-021-03066-4

Eckert, R., Thompson, D. R., Chlus, A. M., Chapman, J. W., Eastwood, M., Bernas, M., ... Green, R. O. (2024). *Aviris-3 l1b calibrated radiance, facility instrument collection.* ORNL Distributed Active Archive Center. Retrieved from https://doi.org/10.3334/ORNLDAAC/2356 doi: 10.3334/ORNLDAAC/2356

Green, R. O., Schaepman, M. E., Mouroulis, P., Geier, S., Shaw, L., Hueini, A., ... Helmlinger, M. (2022, March). Airborne visible/infrared imaging spectrometer 3 (aviris-3). In *2022 ieee aerospace conference (aero)* (p. 1–10). IEEE. Retrieved from http://dx.doi.org/10.1109/AERO53065.2022.9843565 doi: 10.1109/aero53065.2022.9843565

Green, R. O., Sen, A., Pearson, J. C., Mouroulis, P., Patel, S., Sullivan, P., ... Walch, M. (2022). Surface biology and geology (sbg) visible to short wavelength infrared (vswir) wide swath instrument concept. In *2022 ieee aerospace conference (aero)* (p. 1-10). doi: 10.1109/AERO53065.2022.9843676

Hanley, J. A., & McNeil, B. J. (1982, April). The meaning and use of the area under a receiver operating characteristic (roc) curve. *Radiology*, *143*(1), 29–36. Retrieved from http://dx.doi.org/10.1148/radiology.143.1.7063747 doi: 10.1148/radiology.143.1.7063747

Keeley, J. E., & Syphard, A. D. (2019, September). Twenty-first century california, usa, wildfires: Fuel-dominated vs. wind-dominated fires. *Fire Ecology*, *15*(1), 24. Retrieved from https://doi.org/10.1186/s42408-019-0041-0 doi: 10.1186/s42408-019-0041-0

Kerekes, J. (2008, April). Receiver operating characteristic curve confidence intervals and regions. *IEEE Geoscience and Remote Sensing Letters*, *5*(2), 251–255. Retrieved from http://dx.doi.org/10.1109/LGRS.2008.915928 doi: 10.1109/lgrs.2008.915928

Knapp, E. E., Valachovic, Y. S., Quarles, S. L., & Johnson, N. G. (2021, October). Housing arrangement and vegetation factors associated with single-family home survival in the 2018 camp fire, california. *Fire Ecology*, *17*(1). Retrieved from http://dx.doi.org/10.1186/s42408-021-00117-0 doi: 10.1186/s42408-021-00117-0

Kokaly, R. F., Rockwell, B. W., Haire, S. L., & King, T. V. (2007, February). Characterization of post-fire surface cover, soils, and burn severity at the cerro grande fire, new mexico, using hyperspectral and multispectral remote sensing. *Remote Sensing of Environment*, *106*(3), 305–325. Retrieved from http://dx.doi.org/10.1016/j.rse.2006.08.006 doi: 10.1016/j.rse.2006.08.006

Lee, C. M., Glenn, N. F., Stavros, E. N., Luvall, J., Yuen, K., Hain, C., & Schollaert Uz, S. (2022, April). Systematic integration of applications into the surface biology and geology (sbg) earth mission architecture study. *Journal of Geophysical Research: Biogeosciences*, *127*(4), e2021JG006720. Retrieved from https://doi.org/10.1029/2021JG006720 doi: 10.1029/2021JG006720

Maranghides, A., Mell, W., Hawks, S., Wilson, M., Brewer, W., Link, E., ... Ashley, E. (2020). *Preliminary data collected from the camp fire reconnaissance.* Retrieved from http://dx.doi.org/10.6028/NIST.TN.2128 doi: 10.6028/nist.tn.2128

Ochoa, F., Brodrick, P., Okin, G., Roberts, D., Queally, N., Ward-Baranyay, M., ... Green, R. O. (2025, October). Lake fire endmembers. Retrieved from https://doi.org/10.5281/zenodo.17992843 doi: 10.5281/zenodo.17992843

Ochoa, F., Brodrick, P. G., Okin, G. S., Ben-Dor, E., Meyer, T., Thompson, D. R., & Green, R. O. (2025, July). Soil and vegetation cover estimation for global imaging spectroscopy using spectral mixture analysis. *Remote Sensing of Environment*,

324, 114746. Retrieved from http://dx.doi.org/10.1016/j.rse.2025.114746 doi: 10.1016/j.rse.2025.114746

OpenStreetMap contributors. (2025). *Building footprints (openstreetmap data).* OpenStreetMap. Retrieved from https://www.openstreetmap.org/copyright ([Data set])

Quintano, C., Calvo, L., Fernández-Manso, A., Suárez-Seoane, S., Fernandes, P. M., & Fernández-Guisuraga, J. M. (2023, September). First evaluation of fire severity retrieval from prisma hyperspectral data. *Remote Sensing of Environment*, *295*, 113670. Retrieved from http://dx.doi.org/10.1016/j.rse.2023.113670 doi: 10.1016/j.rse.2023.113670

Radeloff, V. C., Helmers, D. P., Kramer, H. A., Mockrin, M. H., Alexandre, P. M., Bar-Massada, A., ... Stewart, S. I. (2018, March). Rapid growth of the us wildland-urban interface raises wildfire risk. *Proceedings of the National Academy of Sciences*, *115*(13), 3314–3319. Retrieved from http://dx.doi.org/10.1073/pnas.1718850115 doi: 10.1073/pnas.1718850115

Riaño, D. (2002, January). Assessment of vegetation regeneration after fire through multitemporal analysis of aviris images in the santa monica mountains. *Remote Sensing of Environment*, *79*(1), 60–71. Retrieved from http://dx.doi.org/10.1016/S0034-4257(01)00239-5 doi: 10.1016/s0034-4257(01)00239-5

Roberts, D., Alonzo, M., Wetherley, E. B., Dudley, K. L., & Dennison, P. E. (2017, January). Integrating scale in remote sensing and gis. In (p. 247-283). CRC Press. Retrieved from http://dx.doi.org/10.1201/9781315373720 doi: 10.1201/9781315373720

Roberts, D., Gardner, M., Church, R., Ustin, S., Scheer, G., & Green, R. (1998, September). Mapping chaparral in the santa monica mountains using multiple endmember spectral mixture models. *Remote Sensing of Environment*, *65*(3), 267–279. Retrieved from http://dx.doi.org/10.1016/S0034-4257(98)00037-6 doi: 10.1016/s0034-4257(98)00037-6

Schmidt, J. (2020). *Vegetation cover and structure loss in four northern california wildfires: Butte, tubbs, carr, and camp* (MPRA Paper). University Library of Munich, Germany. Retrieved from https://EconPapers.repec.org/RePEc:pra:mprapa:104232

Schmidt, J. (2023). *Defensible space, housing density, and diablo-north wind events: Impacts on loss rates for homes in northern california wildfires* (MPRA Paper). University Library of Munich, Germany. Retrieved from https://EconPapers.repec.org/RePEc:pra:mprapa:116166

Swain, D. L., Abatzoglou, J. T., Albano, C. M., Brunner, M. I., Diffenbaugh, N. S., Kolden, C., ... Touma, D. (2025, February). Increasing hydroclimatic whiplash can amplify wildfire risk in a warming climate. *Global Change Biology*, *31*(2). Retrieved from http://dx.doi.org/10.1111/gcb.70075 doi: 10.1111/gcb.70075

Syphard, A. D., & Keeley, J. (2019, September). Factors associated with structure loss in the 2013–2018 california wildfires. *Fire*, *2*(3), 49. Retrieved from http://dx.doi.org/10.3390/fire2030049 doi: 10.3390/fire2030049

Syphard, A. D., Keeley, J. E., Gough, M., Lazarz, M., & Rogan, J. (2022, September). What makes wildfires destructive in california? *Fire*, *5*(5), 133. Retrieved from https://doi.org/10.3390/fire5050133 doi: 10.3390/fire5050133

Tane, Z., Roberts, D., Veraverbeke, S., Casas, A., Ramirez, C., & Ustin, S. (2018, March). Evaluating endmember and band selection techniques for multiple endmember spectral mixture analysis using post-fire imaging spectroscopy. *Remote Sensing*, *10*(3), 389. Retrieved from http://dx.doi.org/10.3390/rs10030389 doi: 10.3390/rs10030389

Tang, W., He, C., Emmons, L., & Zhang, J. (2024, March). Global expansion of wildland-urban interface (wui) and wui fires: insights from a multiyear worldwide unified database (wuwui). *Environmental Research Letters*, *19*(4),

562 044028. Retrieved from http://dx.doi.org/10.1088/1748-9326/ad31da doi:
563 10.1088/1748-9326/ad31da
564 Thompson, D. R., Green, R. O., Bradley, C., Brodrick, P. G., Mahowald, N., Dor,
565 E. B., ... Zandbergen, S. (2024, March). On-orbit calibration and perfor-
566 mance of the emit imaging spectrometer. *Remote Sensing of Environment*, *303*,
567 113986. Retrieved from http://dx.doi.org/10.1016/j.rse.2023.113986 doi:
568 10.1016/j.rse.2023.113986
569 Thompson, D. R., Natraj, V., Green, R. O., Helmlinger, M. C., Gao, B.-C., &
570 Eastwood, M. L. (2018, October). Optimal estimation for imaging spectrom-
571 eter atmospheric correction. *Remote Sensing of Environment*, *216*, 355–373.
572 Retrieved from http://dx.doi.org/10.1016/j.rse.2018.07.003 doi:
573 10.1016/j.rse.2018.07.003
574 Troy, A., Moghaddas, J., Schmidt, D., Romsos, J. S., Sapsis, D. B., Brewer, W., &
575 Moody, T. (2022, May). An analysis of factors influencing structure loss resulting
576 from the 2018 camp fire. *International Journal of Wildland Fire*, *31*(6), 586–598.
577 Retrieved from http://dx.doi.org/10.1071/WF21176 doi: 10.1071/wf21176
578 van Gerrevink, M. J., & Veraverbeke, S. (2021, November). Evaluating the hy-
579 perspectral sensitivity of the differenced normalized burn ratio for assessing fire
580 severity. *Remote Sensing*, *13*(22), 4611. Retrieved from http://dx.doi.org/
581 10.3390/rs13224611 doi: 10.3390/rs13224611
582 Veraverbeke, S., Dennison, P., Gitas, I., Hulley, G., Kalashnikova, O., Katagis,
583 T., ... Stavros, N. (2018, October). Hyperspectral remote sensing of fire:
584 State-of-the-art and future perspectives. *Remote Sensing of Environment*, *216*,
585 105–121. Retrieved from http://dx.doi.org/10.1016/j.rse.2018.06.020 doi:
586 10.1016/j.rse.2018.06.020
587 Veraverbeke, S., Stavros, E. N., & Hook, S. J. (2014, November). Assessing fire
588 severity using imaging spectroscopy data from the airborne visible/infrared imag-
589 ing spectrometer (aviris) and comparison with multispectral capabilities. *Remote*
590 *Sensing of Environment*, *154*, 153–163. Retrieved from http://dx.doi.org/
591 10.1016/j.rse.2014.08.019 doi: 10.1016/j.rse.2014.08.019
592 Wall, T., Steinberg, M., & Shew, D. (2025, March). Community-led rebuilding after
593 the la wildfires. *Nature Sustainability*, *8*(4), 326–326. Retrieved from http://dx
594 .doi.org/10.1038/s41893-025-01531-x doi: 10.1038/s41893-025-01531-x
595 Ward-Baranyay, M., Coleman, R. W., Wronkiewicz, M., Ochoa, F., Sousa, D.,
596 Parker, C. W., ... Brodrick, P. G. (2025, December). *Eaton fire aviris-3 char/ash*
597 *fractional cover mapping.* Zenodo. Retrieved from https://doi.org/10.5281/
598 zenodo.18012266 doi: 10.5281/zenodo.18012266
599 Wolter, P. T., & Townsend, P. A. (2011, February). Multi-sensor data fusion for es-
600 timating forest species composition and abundance in northern minnesota. *Remote*
601 *Sensing of Environment*, *115*(2), 671–691. Retrieved from http://dx.doi.org/10
602 .1016/j.rse.2010.10.010 doi: 10.1016/j.rse.2010.10.010
603 Wronkiewicz, M., Parker, C. W., Ochoa, F., Coleman, R. W., Aguilar, I. N., Okin,
604 G. S., ... Brodrick, P. G. (2025). *Eaton fire ash mapping and analysis: Field*
605 *spectroscopy.* Zenodo. Retrieved from https://zenodo.org/doi/10.5281/
606 zenodo.16538735 doi: 10.5281/ZENODO.16538735

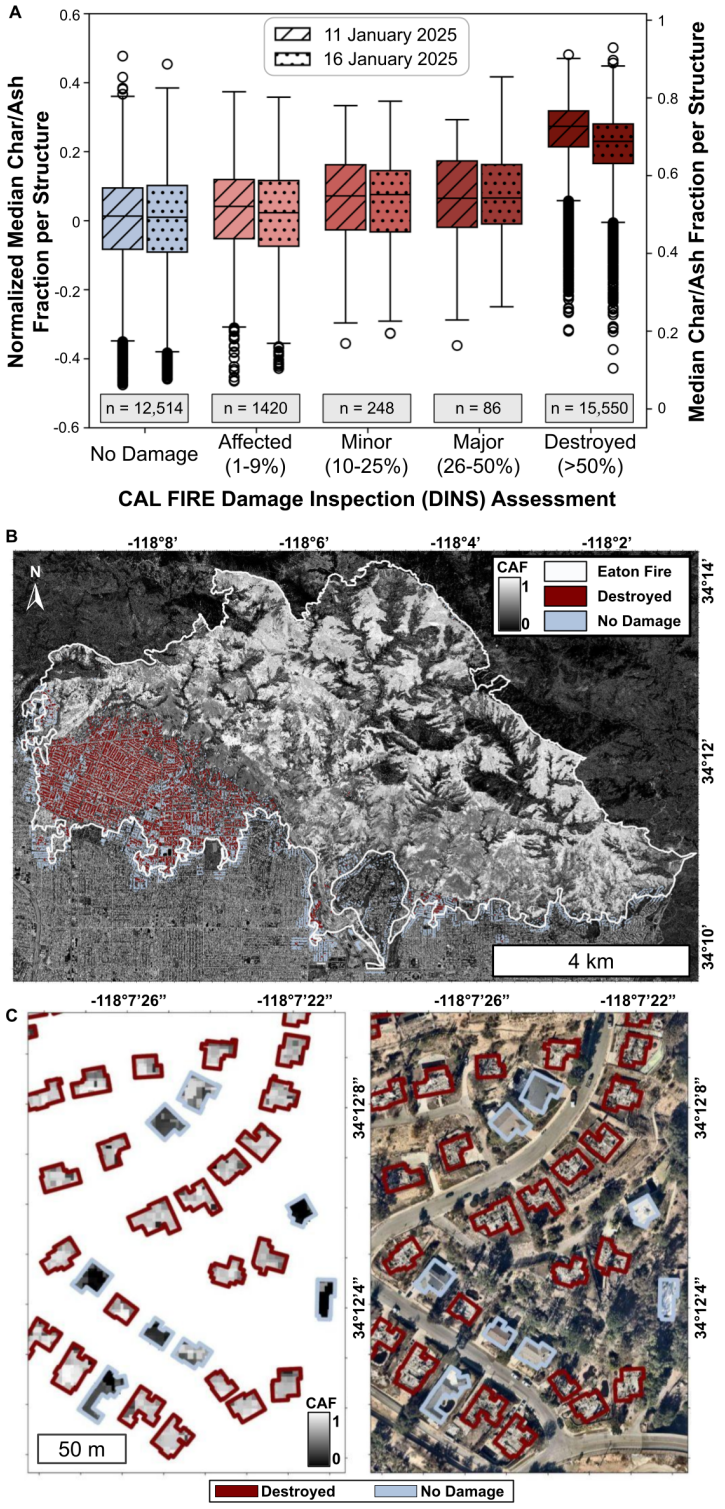

Figure 3. A. Box-and-whisker plot of the median char/ash fraction (CAF) value for structures in the Eaton Fire burn zone categorized by the DINS structural damage categories for two post-fire AVIRIS-3 images acquired on 11 January and 16 January 2025. The left axis depicts CAF values normalized relative to the "No Damage" class, calculated by subtracting the mean "No Damage" CAF value acquired from the same image. Structures with the Inaccessible damage code were omitted due to a small sample size and a lack of information to make a categorical judgment for the validation exercise. The number of pixels within each damage classification is reported. B. Building footprints from the Open Street Maps database, classified with the CAL FIRE Damage Inspection (DINS) database. Only structures classified by DINS as "Destroyed" (red) or "No Damage" (blue) are included. C: Generic CAF values (left) are higher where structures classified as "Destroyed" are located. Multiple pixels sampled each structure, enabling averaged, per-structure estimates of CAF. Nearmap imagery on the right.

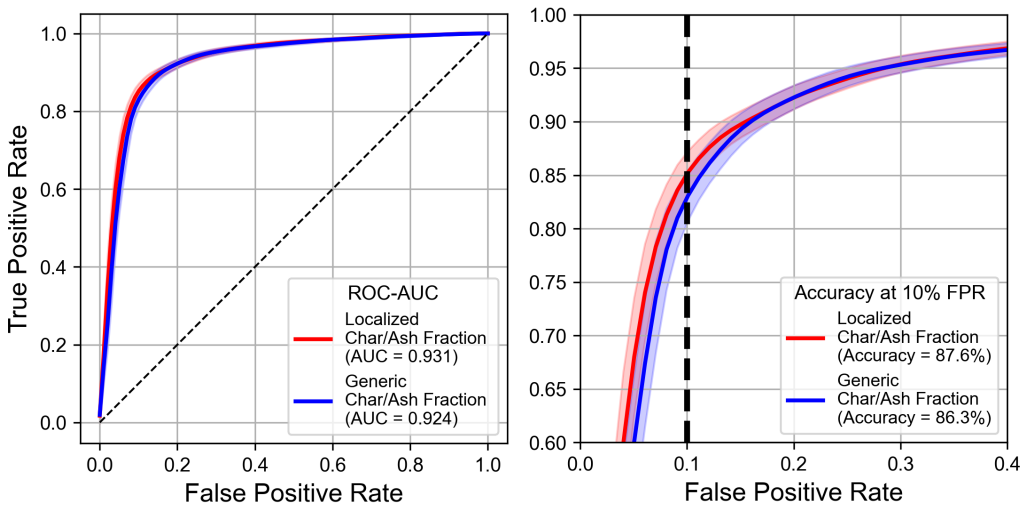

Figure 4. ROC curves were calculated to capture overall model performance and identify fixed thresholds for computing binary accuracy for localized CAF and generic CAF. A bootstrapping approach with 10,000 iterations was applied to generate robust performance evaluations for each CAF metric (see Methods for details). **(A)** Across all bootstrap iterations, the solid line represents the the mean ROC curve, the shaded region represents the standard deviation of the ROC curve, and the legend includes the mean AUC value. The legend includes the mean AUC value over the entire dataset. A dashed 1:1 line is displayed. **(B)** An inset of the upper left portion of the ROC curves shows that the localized CAF metric marginally outperforms the generic CAF metric at low FPRs. A binary classification threshold was derived from 10% FPR (thick dashed line) to generate binary predictions and assess accuracy. Again, localized CAF slightly outperforms generic CAF. The legend includes the mean accuracy at 10% FPR.